

\mathcal{PT} asymmetry in viscous fluids with balanced inflow and outflow

Huidan (Whitney) Yu^{1*}, Xi Chen², Nan Chen¹, Yousheng Xu³, and Yogesh N. Joglekar^{4*}

¹*Department of Mechanical Engineering, Indiana University-Purdue University Indianapolis, Indianapolis, Indiana 46202 USA,*

²*Department of Physics, Zhejiang Normal University, Jinhua 321004, China,*

³*School of Light Industry, Zhejiang University of Science and Technology, Hangzhou 310023, China,*

⁴*Department of Physics, Indiana University-Purdue University Indianapolis (IUPUI), Indianapolis, Indiana 46202 USA*

(Dated: May 22, 2022)

In recent years, open systems with equal loss and gain have been investigated via their symmetry properties under combined parity and time-reversal (\mathcal{PT}) operations. We numerically investigate \mathcal{PT} -symmetry properties of an incompressible, viscous fluid with “balanced” inflow-outflow configurations. We define configuration-dependent asymmetries in velocity, kinetic energy density, and vorticity fields, and find that all asymmetries scale quadratically with the Reynolds number. Our proposed configurations have asymmetries that are orders of magnitude smaller than the asymmetries that occur in traditional configurations at low Reynolds numbers. Our results show that \mathcal{PT} -symmetric fluid flow configurations, which are defined here for the first time, offer a hitherto unexplored avenue to tune fluid flow properties.

Introduction. In a seminal paper [1] Carl Bender and co-authors showed that all eigenvalues of a class of non-Hermitian Hamiltonians are purely real and bounded below. For a Hamiltonian $H_\eta = -\partial_x^2 + x^2(ix)^\eta$, with complex potential $V_\eta(x) = x^2(ix)^\eta$, they showed that when $\eta \geq 0$, the eigenvalue spectrum is purely real whereas for $\eta < 0$, it has a finite number of purely real eigenvalues and the rest occur in complex conjugate pairs. Since then, the properties of Hamiltonians that are invariant under the combined operation of parity and time-reversal (\mathcal{PT}) have been extensively studied in the continuum [2–4] and lattice [5–10] models. For a \mathcal{PT} -symmetric Hamiltonian, the region of parameter space where all eigenvalues ϵ_λ are real, and the eigenfunctions $\psi_\lambda(x)$ are simultaneous eigenfunctions of the combined \mathcal{PT} -operation, is called the \mathcal{PT} -symmetric phase; the emergence of complex conjugate eigenvalues that occur when the system leaves the \mathcal{PT} -symmetric phase is known as \mathcal{PT} -symmetry breaking. This transition is characterized by the asymmetry parameter defined as $\rho_{\mathcal{PT}} = \sum_\lambda \int dx |\psi_\lambda(x) - \psi_\lambda^*(-x)|$. In the \mathcal{PT} -symmetric phase $\rho_{\mathcal{PT}} = 0$, whereas in the \mathcal{PT} -broken phase, this asymmetry parameter is nonzero. The converse of this observation, proven recently, shows that if a non-Hermitian Hamiltonian has purely real spectrum, it must be \mathcal{PT} -symmetric with an appropriately defined parity operator that satisfies $\mathcal{P}^2 = 1$ [11].

Recent experiments have shown that, far from being a mathematical curiosity, \mathcal{PT} -symmetric Hamiltonians naturally represent open, non-equilibrium systems. \mathcal{PT} symmetry breaking has been observed in evanescently coupled optical-waveguides, where light is absorbed in one and amplified in another [12–15], coupled electrical circuits [16], and coupled pendulums [17]. These studies have shown that open systems with spatially separated, balanced sources and sinks undergo a transition from zero asymmetry state to a state with $\rho_{\mathcal{PT}} \neq 0$ [18, 19].

The notions “source-sink”, “gain-loss”, and “inflow-outflow” occur most naturally in fluid systems. However, symmetry properties of viscous flow are not straightforward because the non-linear nature of underlying dynamics implies that superposition principle cannot be used to construct solutions with specific symmetries. Traditionally, viscous flows are driven by upwind flow, pressure difference, or boundary movement and therefore the (steady-state) velocity profiles at the inlet and the outlet are, in general, not identical. In particular, flow symmetry properties in a system with identical inflow and outflow velocity profiles remain unexplored [20]. We note that in the experimentally investigated \mathcal{PT} -symmetric systems [13–16], the gain and loss were confined to electromagnetic fields or energy [17]; for a viscous fluid system, one must distinguish between the mass flow, defined by \mathcal{PT} -symmetric boundary conditions, and the energy flow properties, characterized by the fluid viscosity.

In this paper, we introduce incompressible, viscous fluid configurations with \mathcal{PT} -symmetric boundary conditions and numerically investigate the symmetry properties of resultant steady-state flow using lattice Boltzmann method. We define and calculate the \mathcal{PT} -asymmetries in velocity, kinetic energy density, and vorticity as a function of Reynolds number and distinct configurations of “balanced” inflow and outflow. Our salient results are as follows: i) The asymmetries in balanced configurations are suppressed by orders of magnitude when compared with those in traditional configurations. ii) These asymmetries scale quadratically with the Reynolds number. iii) These results are valid across different balanced inflow and outflow configurations. We emphasize that in all configurations - \mathcal{PT} symmetric or traditional - the total mass flux at the inlet and the outlet are identical. Thus, the phrase “balanced inflow and outflow” implies, in addition, symmetry properties of velocity profile at the inlet and the outlet, as we define below.

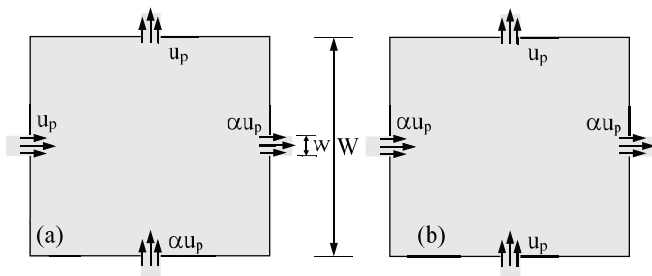


FIG. 1. Two distinct balanced inflows and outflows possible in a square geometry. Panel (a) shows a \mathcal{PT} -invariant configuration where parity \mathcal{P}_O corresponds to reflection across the square diagonal. Panel (b) shows a \mathcal{PT} -invariant configuration where parity \mathcal{P}_E corresponds to reflection through the origin. We use a parabolic velocity profile $u_x(y) = u_p[1 - (2y/w)^2]\theta(w - 2|y|)$ at the inlet and outlet, where $\theta(y)$ is the Heaviside function.

Model and Formalism. We start with the definition of \mathcal{PT} -symmetry for fluids, motivated by the notion of balanced inflow and outflow. Consider two square geometries of width W , with inflows/outflows of width w and origin of the co-ordinate system at the center of the square. Both panels, (a) and (b), in Fig. 1 show “balanced” situations, but correspond to different definitions of parity operator. The left-hand panel (a) shows boundary velocity profile that is invariant under \mathcal{PT} -transformations where the parity operator is defined as $\mathcal{P}_O(x, y) = (-y, -x)$. This (odd) parity operation, a reflection in the southeast-to-northwest diagonal, satisfies $\det \mathcal{P}_O = -1$ and $\mathcal{P}_O^2 = 1$. Under this transformation, the velocity field inside the square changes as $\mathcal{P}_O \mathcal{T}(u_x, u_y) = (u_y, u_x)$.

The right-hand panel (b) shows boundary velocity profiles that are invariant under \mathcal{PT} -transformations where the even “parity” operator is given by $\mathcal{P}_E(x, y) = (-x, -y)$. In contrast to the standard definition of parity in even dimensions, $\det \mathcal{P}_E = 1$ since it is just a two-dimensional π -rotation. The velocity field remains unchanged under this transformation, $\mathcal{P}_E \mathcal{T}(u_x, u_y) = (u_x, u_y)$. Note that one-dimensional inflow-outflows are special cases of this geometry with $\alpha = 0$ (vertical) and $\alpha^{-1} = 0$ (horizontal). We point out that apart from the inflow and outflow locations, fluid velocities at all other points on the boundary vanish due to no-slip condition required by a viscous fluid, and that for $\alpha = \{0, 1, \infty\}$, the boundary conditions are \mathcal{PT} -symmetric with respect to both parity operators \mathcal{P}_O and \mathcal{P}_E .

We define the dimensionless \mathcal{PT} asymmetry in the steady-state velocity field $\mathbf{u}(\mathbf{r})$ for panel (a) configuration as

$$\rho_O^u = \frac{1}{2W^2 u_p^2} \int d\mathbf{r} [\mathbf{u}(\mathcal{P}_O \mathbf{r}) - \mathcal{P}_O \mathcal{T} \mathbf{u}(\mathbf{r})]^2, \quad (1)$$

and corresponding definitions for asymmetry ρ_O^k in the kinetic energy density $T(\mathbf{r}) = \rho \mathbf{u}(\mathbf{r})^2 / 2$ where ρ is the

fluid density, and the asymmetry ρ_O^ω for the pseudo-scalar vorticity field $\omega_z(\mathbf{r}) = \nabla \times \mathbf{u}(\mathbf{r})$. Eq.(1) is applicable for $\alpha \leq 1$ whereas when $\alpha \geq 1$, the prefactor in front of the integral changes to $[2W^2(\alpha u_p)^2]^{-1}$ so that the equivalence between $\alpha \leftrightarrow \alpha^{-1}$ and the exchange of axes, $x \leftrightarrow y$, is preserved. For configurations in panel (b), corresponding asymmetries ρ_E^i are defined using the even “parity” operator \mathcal{P}_E instead of the odd parity operator \mathcal{P}_O . Note that, by construction, the boundary contribution to the asymmetry in all “balanced” inflow and outflow scenarios is zero.

The fluid flow is governed by the Navier-Stokes equation

$$\partial_t \mathbf{u} + (\mathbf{u} \cdot \nabla) \mathbf{u} = -\nabla p / \rho + \nu \nabla^2 \mathbf{u}, \quad (2)$$

where ν is the kinematic viscosity, and $\mathbf{u}(\mathbf{r}, t)$ and $p(\mathbf{r}, t)$ are the velocity and pressure fields respectively. The Reynolds number is defined as $\text{Re} = u_p w / \nu$ for $\alpha \leq 1$ ($\text{Re} = \alpha u_p w / \nu$ for $\alpha \geq 1$). We use kinetic-based lattice Boltzmann method (LBM) to solve Eq.(2) through a validated code. Originated from lattice gas automata, the LBM has developed into a promising numerical scheme for modeling viscous fluids, with physical and computation advantages to deal with flow complexity [21, 22]. The fundamental idea of the LBM is to construct simplified kinetic models for spatially and temporally discretized distribution functions. The evolution of these functions incorporates the physics of mesoscopic processes so that the coarse-grained observables obey desired macroscopic equations [23]. The lattice Boltzmann equation reads

$$f_\beta(\mathbf{r} + \mathbf{e}_\beta \delta_t, t + \delta_t) = f_\beta(\mathbf{r}, t) - [f_\beta(\mathbf{r}, t) - f_\beta^{\text{eq}}(\mathbf{r})] / \tau \quad (3)$$

where $f_\beta(\mathbf{r}, t)$ ($\beta = 0, \dots, 8$) are the single-particle distribution functions with nine discrete velocities $\mathbf{e}_\beta = \{0, \pm \hat{x}, \pm \hat{y}, \pm \hat{x} \pm \hat{y}\}$ used in the two-dimensional 9-bit square lattice model [23], $f_\beta^{\text{eq}}(\mathbf{r})$ are the equilibrium distribution functions, τ is the relaxation time determined by molecular collisions, and in turn, it determines the viscosity of the fluid. The hydrodynamic velocity field is given by

$$\mathbf{u}(\mathbf{r}) = \frac{1}{\rho} \sum_{\beta=0}^8 \mathbf{e}_\beta f_\beta(\mathbf{r}) = \sum_{\beta} \mathbf{e}_\beta f_\beta(\mathbf{r}) / \sum_{\beta} f_\beta(\mathbf{r}). \quad (4)$$

We use bounce-back boundary condition at the walls to ensure no-slip, and generalized bounce-back boundary condition [24] at the inlet and the outlet with a parabolic velocity profile having a centerline velocity u_p or αu_p .

Numerical Results. Let us start with the steady-state velocity profiles obtained for different configurations to get a feel for typical velocity fields (left-hand side in Fig. 2). Panel (a) has $\alpha = 0$ and shows a small velocity asymmetry as can be visually checked by comparing velocities

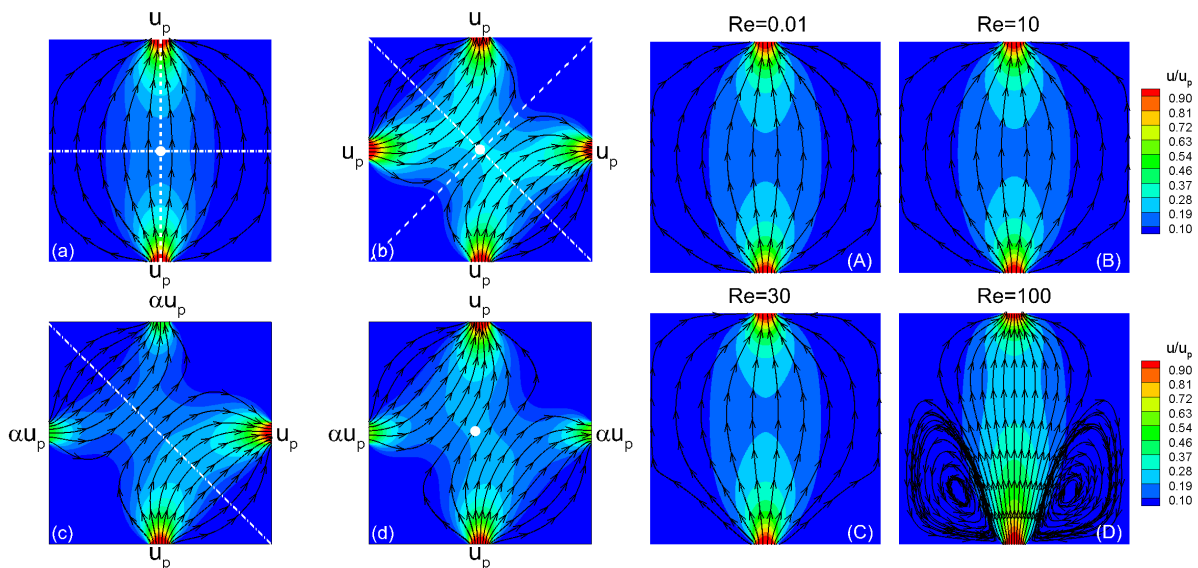


FIG. 2. Left figure: Typical steady-state velocity fields $\mathbf{u}(\mathbf{r})$ for different “balanced” geometries with $w/W = 0.1$; a small $\text{Re} = 0.01$; and $\alpha = 0$ (a), $\alpha = 1$ (b), $\alpha = 0.58$ (c) and (d). Note that due to the geometry, the velocity profile in (a) satisfies $u_x(-x, y) = -u_x(x, y)$ and $u_y(-x, y) = u_y(x, y)$, and in (c) satisfies $u_x(y, x) = u_y(x, y)$ and $u_y(y, x) = u_x(x, y)$ exactly. Right figure: For configuration in panel (a), dependence of the steady-state $\mathbf{u}(\mathbf{r})$ as a function of Reynolds number. For $\text{Re} = 0.01$ (A), the velocity profile is essentially symmetrical; for $\text{Re} = 10$ (B) and $\text{Re} = 30$ (C), the asymmetry is visible. When $\text{Re} = 100$ (D) the asymmetry is accentuated by the emergence of vortices near the inflow region that are absent near the outflow region.

at points $\pm \mathbf{r}$. When $\alpha = 1$, panel (b), the resultant velocity profile is reflection-symmetric about southwest-to-northeast diagonal, shown by the white dashed line, but has a weak asymmetry about the other diagonal, shown by white dash-dotted line. Panel (c) with $\alpha = 0.58$ has a weak asymmetry across the diagonal denoted by white dash-dotted line and Panel (d) shows the complementary configuration. Note that for panels (a), (b), and (d), the asymmetry ρ_E associated with reflection through the origin, shown by the central white dot, is relevant; for panels (b) and (c), the asymmetry ρ_O associated with reflection along the diagonal, shown by white dash-dotted line, is relevant.

The right-hand side in Fig. 2 shows the steady-state velocity field for a vertical flow ($\alpha = 0$) as a function of the centerline speed u_p , or equivalently, the Reynolds number Re . As Re changes over four decades, the asymmetry in the velocity field at points $\pm \mathbf{r}$ also increases. When $\text{Re} = 0.01$ (A), the even-parity asymmetry is barely noticeable; for $\text{Re} = 10$ (B) and $\text{Re} = 30$ (C), it is clearly visible; for $\text{Re} = 100$ (D), the asymmetry is accentuated by the emergence of vortices near the inflow region that are absent near the outflow region. Note that the velocity field satisfies $u_x(-x, y) = -u_x(x, y)$ and $u_y(-x, y) = u_y(x, y)$ exactly, and thus guarantees that the net vorticity of the velocity field vanishes.

Next, we consider the quantitative scaling of the relevant asymmetries with system parameters. The left-hand side of Fig. 3 shows the typical scaling of even-parity asymmetries $\rho_E(\text{Re}, \alpha)$ with Reynolds number Re

for different values of $\alpha \leq 1$. Panel (A) shows that the *velocity asymmetry scales quadratically with the Reynolds number over four decades*, $\rho_E^u = A^u(\alpha)\text{Re}^2$; panels (B) and (C) show that the asymmetries in kinetic energy density and vorticity also scale quadratically with the Reynolds number, $\rho_E^k = A^k(\alpha)\text{Re}^2$ and $\rho_E^\omega = A^\omega(\alpha)\text{Re}^2$. Panel (D) shows that the prefactor functions for the even-asymmetry $A^i(\alpha)$ increase monotonically with α for $0 \leq \alpha \leq 1$. These results are valid for different inlet sizes or boundary velocity profiles.

The right-hand side of Fig. 3 compares the asymmetries in balanced-outflow model (BO) with those of a traditional model with fully-developed-outflow (FDO) at the outlet. Panels (a) and (b) show the speed profiles at $\text{Re} = 0.01$ and $w/W = 0.1$ for the two cases respectively. Panel (c) shows the clear difference between the steady-state velocity profile $u_x(x, y)$ at the outlet for the balanced-outflow case (solid line) and the fully-developed-outflow case (dashed line). These differences between the \mathcal{PT} -symmetric and traditional models are quantified in panel (d). It shows that in the \mathcal{PT} -symmetric case, as before, the relevant odd asymmetries scale quadratically with the Reynolds number (lines with open symbols). In a sharp contrast, however, *asymmetries in traditional models with fully-developed-outflow are orders of magnitude larger* and, over three decades, are mostly insensitive to the Reynolds number (lines without symbols). These results show that \mathcal{PT} -symmetric inflow-outflow configurations strongly suppress observable asymmetries compared to their traditional counter-

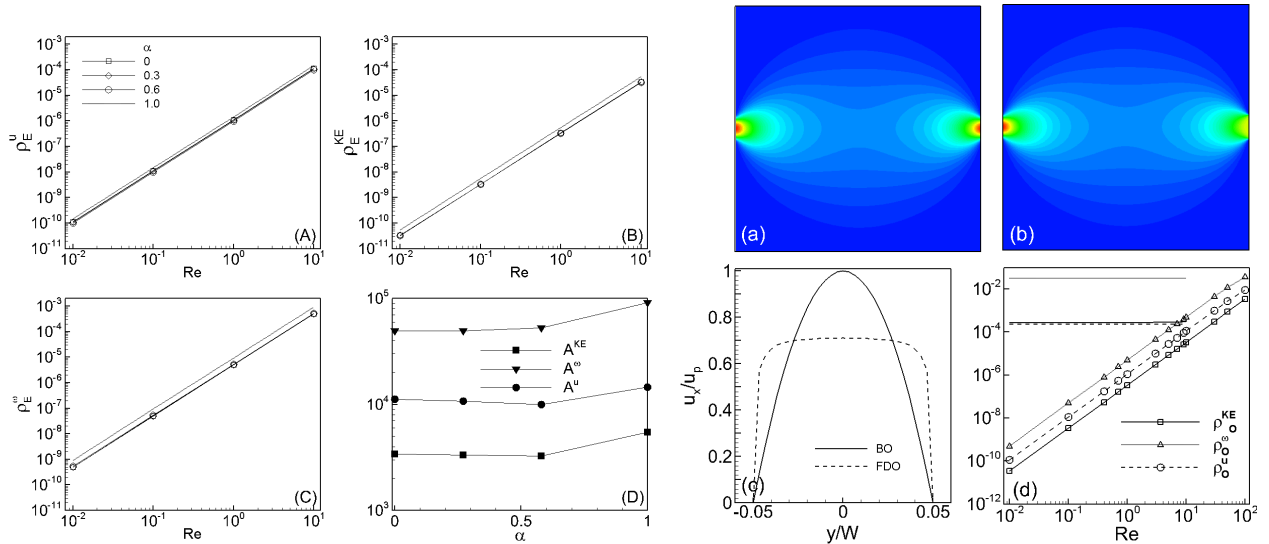


FIG. 3. Left figure: For panel (d) of Fig. 2, the dependence of even-parity asymmetries in velocity (A), kinetic energy density (B), and the vorticity (C) as a function of α shows that they scale quadratically with the Reynolds number, $\rho_E^i(\text{Re}, \alpha) = A^i(\alpha)\text{Re}^2$ for $i = u, k, \omega$. Panel (D) shows the behavior of $A^i(\alpha)$ for $0 \leq \alpha \leq 1$. Right figure: Comparisons between balanced-outflow (panel a) and fully-developed-outflow (panel b) speed profiles at $\text{Re} = 0.01$ and inlet size $w/W = 0.1$. Panel (c) shows the clear difference between velocity profiles $u_x(x = W/2, y)$ at the outlet for BO boundary condition (solid line; panel a) and FDO boundary condition (dashed line; panel b). Panel (d) shows that $\rho_O^i(\text{Re})$ for the BO case (lines with symbols) scale as Re^2 , whereas those for the FDO case (lines without symbols) are orders of magnitude larger.

parts.

Discussion. In this paper, we have developed the formalism of \mathcal{PT} -symmetric inflow-outflow configurations for incompressible viscous fluids. Motivated by the loss of reciprocity, $\rho_{PT} \neq 0$, as the signature of \mathcal{PT} -symmetry breaking, we have defined configuration-dependent asymmetry functions $\rho(\text{Re}, \alpha)$ for fluid velocity profile, kinetic energy density, and vorticity. Although the nonlinearities due to convective acceleration, the $(\mathbf{u} \cdot \nabla)\mathbf{u}$ term in the Navier-Stokes equation, make it difficult to predict the symmetry properties of these variables, we have found that *all asymmetries scale quadratically* with the Reynolds number over a wide range of geometries and boundary velocity profiles. We emphasize here that $\rho^u(\text{Re})$ and $\rho^\omega(\text{Re})$ involve the square of velocity, whereas the kinetic energy density involves its fourth power. Thus, their identical quadratic scaling is cannot be ascribed to the functional form of the asymmetry. Similarly, the virtual independent of these asymmetries on the Reynolds number in the fully-developed-outflow case implies that this effect cannot be purely ascribed to the convective acceleration term.

Our results show that solutions of incompressible, viscous flow problems with \mathcal{PT} -symmetric boundary conditions are highly symmetrical, particularly at low Reynolds numbers $\text{Re} \leq 1$, compared to their counterparts with traditional boundary conditions. This increased symmetry of the steady-state solutions implies that such configurations are, generically, robust against the formation of vortices than the traditional configura-

tions. Our results thus lay the foundation for the study of \mathcal{PT} -symmetric fluid systems. Note that the lack of a finite, nonzero threshold for the asymmetry functions is due to the purely dissipative, viscous term and nonlinearities in Eq.(2); this is in contrast with the experiments on \mathcal{PT} -symmetric systems [13–17] where both dissipation and amplification are present. Formally, an exactly \mathcal{PT} -symmetric fluid system requires an antisymmetric viscosity $\nu(\mathcal{P}\mathbf{r}) = -\nu(\mathbf{r})$. Since this is physically impossible, one can consider a system where viscosity has an antisymmetric component $\nu(x, y) = \nu_0 + \text{sign}(x)\Delta\nu$. This location-dependent enhancement or suppression of viscosity is possible in ferrofluids [25, 26]. Thus, investigation of such a system may provide an example of truly \mathcal{PT} -symmetric fluid system. We also note that viscous fluid flow with porous walls has been extensively studied, although such problems do not have “balanced inflow and outflow” boundary conditions [27–29].

This work raises a number of questions: Does the quadratic scaling of asymmetry persist when the flow become transitional or turbulent at higher Reynolds numbers? How does the asymmetry scale in a rectangular geometry? Does the onset of turbulence occur at the same Reynolds number for a “balanced” geometry as it does for fully-developed-flow boundary conditions? Answers to these questions may inspire innovative flow control techniques, with implications to a wide variety of fields.

This work was supported by RSFG IUPUI (HY), National Nature Science Foundation of China (NNSFC) 10972208 (HY), and NSF-DMR 1054020 (YJ).

-
- * whyu@iupui.edu, yojoglek@iupui.edu
- [1] C.M. Bender and S. Boettcher, *Phys. Rev. Lett.* **80**, 5243 (1998).
- [2] C.M. Bender, D.C. Brody, and H.F. Jones, *Phys. Rev. Lett.* **89**, 270401 (2002).
- [3] For a review, see C.M. Bender, *Rep. Prog. Phys.* **70**, 947 (2007) and references therein.
- [4] A. Mostafazadeh, *Int. J. Geom. Meth. Mod. Phys.* **7**, 1191 (2010) and references therein.
- [5] O. Bendix, R. Fleischmann, T. Kottos, and B. Shapiro, *Phys. Rev. Lett.* **103**, 030402 (2009).
- [6] L. Jin and Z. Song, *Phys. Rev. A* **80**, 052107 (2009).
- [7] Y.N. Joglekar, D. Scott, M. Babbey, and A. Saxena, *Phys. Rev. A* **82**, 030103(R) (2010).
- [8] M. Znojil, *Phys. Rev. A* **82**, 052113 (2010).
- [9] M. Znojil, *Phys. Lett. A* **375**, 3435 (2011).
- [10] Y.N. Joglekar and A. Saxena, *Phys. Rev. A* **83**, 050101(R) (2011).
- [11] C.M. Bender and P.D. Manheim, *Phys. Lett. A* **374**, 1616 (2010).
- [12] A. Guo, G.J. Salamo, D. Duchesne, R. Morandotti, M. Volatier-Ravat, V. Aimez, G.A. Siviloglou, and D.N. Christodoulides, *Phys. Rev. Lett.* **103**, 093902 (2009).
- [13] C.E. Rüter, K.G. Makris, R. El-Ganainy, D.N. Christodoulides, M. Segev, and D. Kip, *Nat. Phys.* **6**, 192 (2010).
- [14] L. Feng, M. Ayache, J. Huang, Y.-L. Xu, M.-H. Lu, Y.-F. Chen, Y. Fainman, and A. Scherer, *Science* **333**, 729 (2011).
- [15] A. Regensburger, C. Bersch, M.-A. Miri, G. Onishchukov, D.N. Christodoulides, and U. Peschel, *Nature* **488**, 167 (2012).
- [16] J. Schindler, A. Li, M.C. Zheng, F.M. Ellis, and T. Kottos, *Phys. Rev. A* **84**, 040101(R) (2011).
- [17] C.M. Bender, B.K. Berntson, D. Parker, and E. Samuel, *Am. J. Phys.* **81**, 173 (2013).
- [18] T. Kottos, *Nat. Phys.* **6**, 192 (2010).
- [19] M.C. Zheng, D.N. Christodoulides, R. Fleischmann, and T. Kottos, *Phys. Rev. A* **82**, 010103(R) (2010).
- [20] An example of a non-viscous flow with a balanced source and sink is Rankine oval; it has zero asymmetry. See, for example, F.M. White, *Fluid Mechanics* (McGraw Hill, New York, NY 2010).
- [21] S. Chen and G. D. Doolen, *Ann. Rev. Fluid Mech.* **30**, 329 (1998).
- [22] C. K. Aidun and J. R. Clausen, *Ann. Rev. Fluid Mech.* **42**, 439 (2010).
- [23] X. He and L.-S. Luo, *Phys. Rev. E* **55**, R6333 (1997); *ibid* **56**, 6811 (1997).
- [24] L.-S. Luo, *Phys. Rev. E* **62**, 4982 (2000).
- [25] M.I. Shliomis and K.I. Morozov, *Phys. Fluids* **6**, 2855 (1994).
- [26] J.-C. Bacri, R. Perzynski, M.I. Shliomis, and G.I. Burde, *Phys. Rev. Lett.* **75**, 2128 (1995).
- [27] A.S. Berman, *J. App. Phys.* **24**, 1232 (1953).
- [28] I. Proudman, *Fluid Mech.* **9**, 593 (1960).
- [29] S.M. Cox, *J. Fluid. Mech.* **227**, 1 (1991).